Spark plasma sintering of Stellite®-6 superalloy

Kiani Khouzani, M.; Bahrami, A.; Yazdan Mehr, M.

DOI
10.1016/j.jallcom.2018.12.186

Publication date
2019

Document Version
Accepted author manuscript

Published in
Journal of Alloys and Compounds

Accepted Manuscript

Spark plasma sintering of Stellite®-6 superalloy

M. Kiani Khouzani, A. Bahrami, M. Yazdan Mehr

PII: S0925-8388(18)34742-X

DOI: https://doi.org/10.1016/j.jallcom.2018.12.186

Reference: JALCOM 48827

To appear in: *Journal of Alloys and Compounds*

Received Date: 5 August 2018

Revised Date: 4 December 2018

Accepted Date: 13 December 2018

Please cite this article as: M. Kiani Khouzani, A. Bahrami, M. Yazdan Mehr, Spark plasma sintering of Stellite®-6 superalloy, *Journal of Alloys and Compounds* (2019), doi: https://doi.org/10.1016/j.jallcom.2018.12.186.

Spark plasma sintering of Stellite®-6 superalloy

M. Kiani Khouzani[1], A. Bahrami[1], M. Yazdan Mehr[2]*

[1] *Department of Materials Engineering, Isfahan University of Technology, Isfahan 84156-83111, Iran*
[2] *Faculty EEMCS, Delft University of Technology, Mekelweg 4, 2628 CD Delft, The Netherlands*

* Corresponding Author: m.yazdanmehr@tudelft.nl

Abstract:

This paper aims at studying microstructure and mechanical properties of spark plasma sintered (SPSed) Stellite®-6 cobalt-based superalloy. SPS is a sintering technique, based on a relatively fast resistance heating using a pulsed current. Fast sintering process, associated with minimum grain growth, results in excellent mechanical properties. Samples were sintered at temperatures ranging from 950 to 1100°C. Microstructure of samples were studied using scanning electron microscope (SEM), energy-dispersive X-ray spectroscope (EDS), X-Ray diffraction (XRD), and optical microscope. Hardness as well as room and high temperature compression tests were used to evaluate the effects of sintering temperature and duration on the mechanical properties of SPSed samples. Results show that optimum mechanical properties can be obtained after sintering at 1050ºC for 10 min. The correlation between sintering parameters, microstructure, and mechanical properties are discussed.

Keywords: Spark plasma sintering; Stellite®-6 alloy; Superalloy; Microstructure; Mechanical properties

1. Introduction

Superalloys are high performance strategic alloys that exhibit superior oxidation resistance, excellent high temperature erosion-corrosion resistance, and very good high temperature mechanical properties [1]. These alloys are widely used in different high temperature industrial applications. Amongst different grades of superalloys, Stellite is a cobalt-based grade, that shows optimum combination of wear resistance, oxidation resistance, and mechanical properties. More importantly, alloys in this grade have proven to maintain their properties in extreme temperature conditions. Stellite is essentially a Co-based alloy that mainly contains alloying elements, such as chromium (Cr), tungsten (W), and carbon (C). This alloy owes its excellent mechanical properties to solid solution strengthening, mostly achieved by dissolution of Cr in the matrix. Cr as the main alloying element also reacts with C to form complex and inter-dendritic carbides. Chromium carbide particles enhance the oxidation/corrosion resistance of the alloy as well as its high temperature strength. The other alloying elements, W, is also a strong carbide forming element. The distribution, morphology, and size of carbide particles greatly influences the mechanical properties of the alloy. That is why controlling processing conditions during manufacturing plays a prominent role in final characteristic of the alloy [2-7]. Depending on the composition and the microstructure, Stellite alloys can be used in different applications, including machine parts, gas turbines, hardfacing, valve seats, implants, and industrial saws [2]. Different petroleum, gas, and pharmaceutical industries benefit from Stellite alloys [8]. Also, different grades of Stellite alloys are widely used for repair purposes, i.e. in repair welding of turbine blades and nozzles.

Different manufacturing methods are employed to make components from Stellite alloys among which casting, welding, and powder metallurgy routes are most widely used. The latter has the advantage of being performed in solid state, inferring that there is no need to deal with typical casting and solidification problems such as segregation, porosity, coarse grain

structure, dendritic structure, and interconnected brittle eutectic carbide network between the dendrites [9,10]. In addition to that, powder metallurgy has more controllability over the microstructure-properties relationships. Numerous researchers have studied processing parameters-microstructure-properties relationship of Stellite alloy, fabricated by hot isostatic pressing (HIP) and powder injection molding (PIM) [9,11]. But, to our knowledge, there are very limited studies on the spark plasma sintering (SPS) of this alloy [12]. SPS has recently emerged as a powder metallurgy technique, with high-speed compaction characteristic. Overall it is a fast, near net-shape, low cost, and flexible method [13]. SPS essentially consists of high temperature pressing (20-100 MPa) of powders in a graphite die under simultaneous flow of current pulses. As mentioned before, it is considered as a fast P/M technique, which gives the possibility of consolidation with minimum grain growth, which in turn results in good mechanical properties [14]. In comparison to other more conventional sintering techniques, SPS has advantages of being conducted at comparatively lower sintering temperatures with relatively short sintering time. SPSed parts exhibit higher sintered densities, limited grain growth and minimal material loss during sintering, thereby making this technique promising with great potential [13]. In SPS technology, raw or mechanically alloyed ceramic, metallic, functional, oxide, and composite powders can be consolidated [15-19]. Rarely is there any comprehensive study, which addresses the correlation between the SPS parameters and the microstructure and mechanical properties of SPSed alloy. This study aims at optimization of SPS parameter to achieve highest possible mechanical properties. The experimental studies in this investigation mainly focus on the effects of SPS processing parameters (i.e., sintering temperature and sintering time) on the microstructure and mechanical properties of Stellite®-6 alloy. This specific alloy is the most widely used alloy in Stellite grade, with its application mostly being in P/M-made parts.

2. Materials and Methods

Cobalt-based Stellite®-6 superalloy powder with the average particle size of 35 μm was used in this study. Fig. 1 depicts SEM images of the powder, showing that particles have spherical morphologies with a very narrow particle size distribution, which is typical of atomized powders. Dendritic structure can be seen on particles in Fig. 1, which is a result of casting and solidification during manufacturing. Table 1 gives the chemical composition of the alloy.

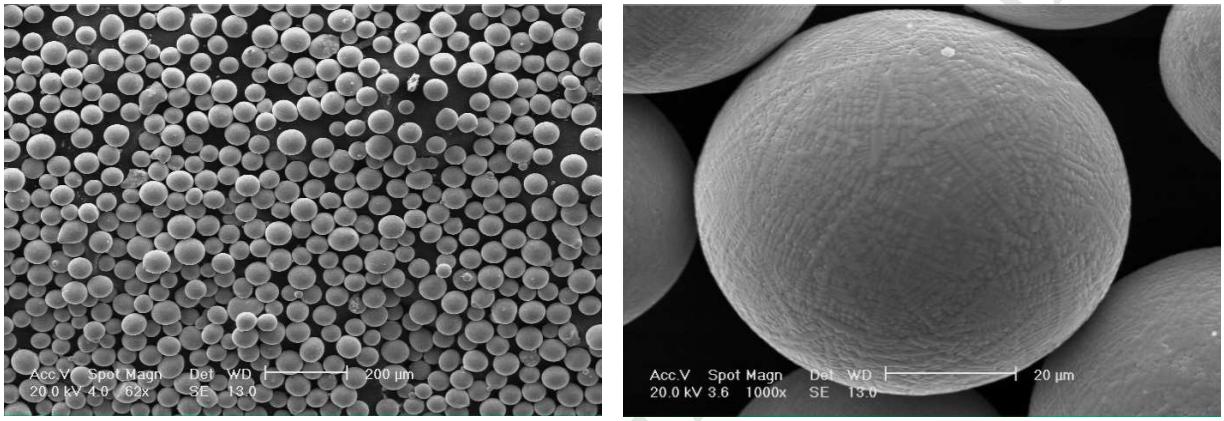

Fig. 1. SEM (SE) image of Stellite®-6 superalloy powder

Table 1. Chemical composition of Stellite®-6 superalloy powder

Elements	Co	Cr	W	Fe	Ni	C	Si	Mn	Mo	P	S
Weight %	62.9	24.5	4.3	2.7	1.6	1.15	1.02	1.17	0.55	0.008	0.004

All experiments were performed by the SPS machine KPF vacuum technology. The powder is poured in a graphite die with a cylindrical cavity with diameter 1.5 cm. The radial punches' surface and the inner surface of the die were shielded with a graphite foil (0.2 mm in thickness) to avoid sticking of the SPSed part to the die. An axial pressure of 50 MPa was applied throughout the heating stage under a controlled Ar atmosphere. Effects of sintering time on the microstructure of the SPSed parts were investi

gated by changing sintering time at 1050˚C. To study the effects of sintering temperature on the microstructure and mechanical properties of SPSed parts, the specimens were heated to 950, 1000, 1050, 1075 and 1100°C at a rate of 150˚C/min and held at these temperatures for

10 min and cooled down at SPS machine. After removing the sintered specimens from the graphite die, the samples were cut, ground, polished, and etched for metallographic examination. The etchant for this alloy was 200 ml HCl (32%), 5 gr $FeCl_3$ and 5 ml nitric acid (65%) solution. The microstructure of specimens was examined by scanning electron microscopy (SEM), connected to an energy dispersive X-ray spectroscopy (EDS). X-Ray Diffractometer (XRD) analyses were carried out on initial powders as well as sintered samples, using Cu K-alpha radiation for phase identification. Grain size was estimated from XRD patterns, using Scherrer formula [20]:

$$D = \frac{0.9\lambda}{\beta(2\theta)Cos\theta} \quad (1),$$

The densities of the sintered samples were measured according to the Archimedes' principle. Compression tests were performed on cylindrical samples of 5 mm diameter with approximate height of 7.5 mm at room temperature and at 650˚C. For high temperature compression test samples were pre-heated at 650˚C for 15 min. The hardness measurements were conducted using Vickers hardness through the application of 100 gf load for 10 s (Micro hardness tester/MICROMET-S101 made in Mitutoyo Japan). Sub-size Charpy-U notch samples for impact toughness testing were prepared according to STP1418 standard [21]. The samples of 4 mm × 3 mm × 27 mm having 1 mm depth with a 60° notch angle and 0.25 notch tip radius were machined with electrodischarge machining technique from sintered samples.

3. Results and discussion

3.1. Microstructure of spark plasma sintered samples

Figure 2 shows the effects of sintering time on the size and morphology of porosities in the sample, SPSed at 1050ºC for 2, 5, 10, and 15 min. Porosity percentage and density are key factors, affecting the mechanical properties of metallic P/Med alloys. It is a basic fact that the higher the sintering temperature, the higher is the final density of the consolidated part.

Higher density means lower internal microstructural discontinuities and defects, with both having negative implications for the mechanical properties and the integrity of P/Med powders. In order to evaluate the effects of sintering time on the densification behavior of Stellite-6, SPSed specimens were polished and studied with optical microscope. As can be seen in Fig. 2, after 2 minutes, particles are at the early stage of sintering, with particles being connected. Further holding up to 5 min is accompanied with the formation of diffusion necks between particles. After 10 minutes of holding, there is no sign of isolated rounded particles. Some isolated porosities are still left in the microstructure though. Further increase in holding time up to 15 min does not show any significant change in the area fraction of porosities, implying that 10 min is the optimum holding time. Shorter holding times result in the formation of a microstructure in which porosity is the dominant feature and longer holding time does not deliver a microstructure with a reduced porosity. Longer holding time increases the possibility of grain growth and carbide coarsening, with both having negative implications for the mechanical properties of the alloy. Fig. 3 shows the comparison between carbide size in samples, sintered for 10 and 15 minutes. Carbides are clearly coarser in the latter. Controlling grain/carbide size is vital when it comes to controlling mechanical and physical properties of materials. Microstructures with finer carbides generally improve the creep, tensile, and fatigue properties of high temperature alloys in severe service conditions. Increasing sintering temperature and holding time, if not properly well planned, result in coarse grain/carbide microstructures [22, 23].

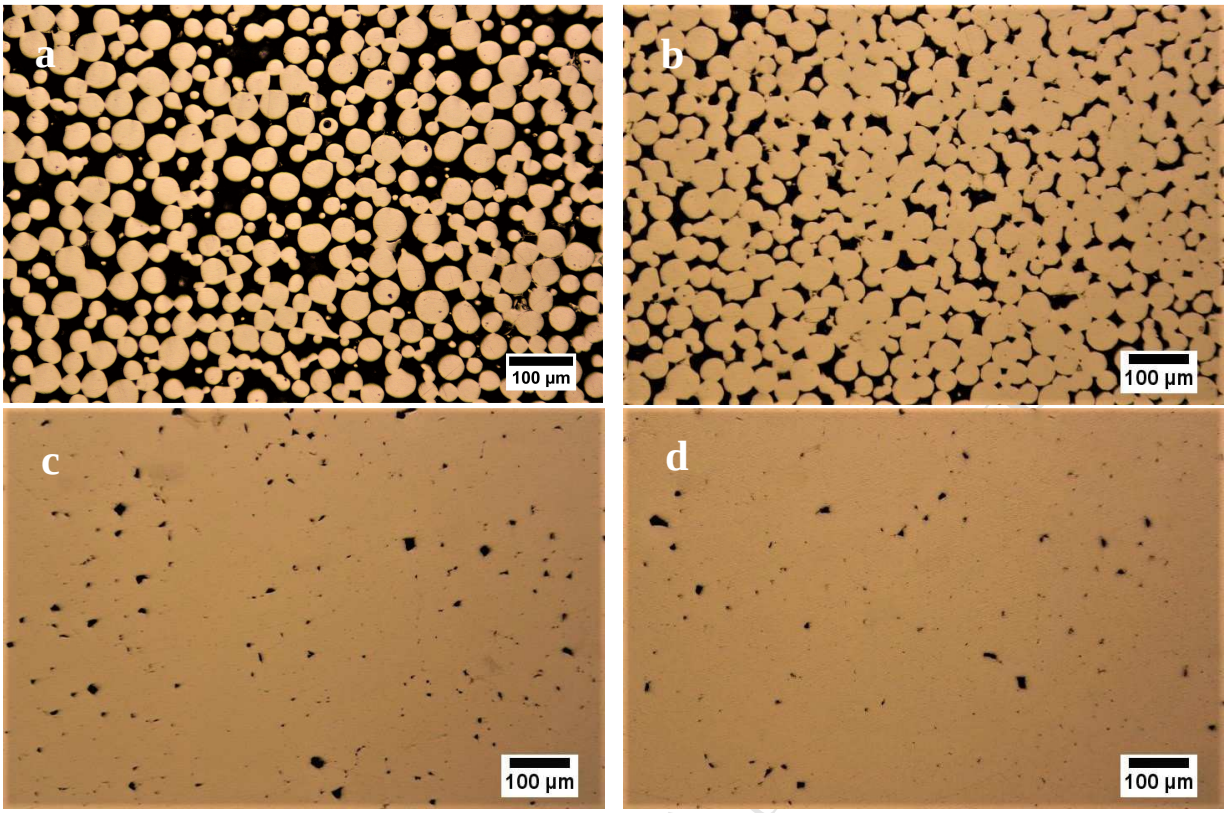

Fig. 2. Effects of sintering time on the morphology and distribution of porosities in samples, SPSed at 1050ºC for a) 2, b) 5, c) 10, and d) 15 min holding (sintering) time

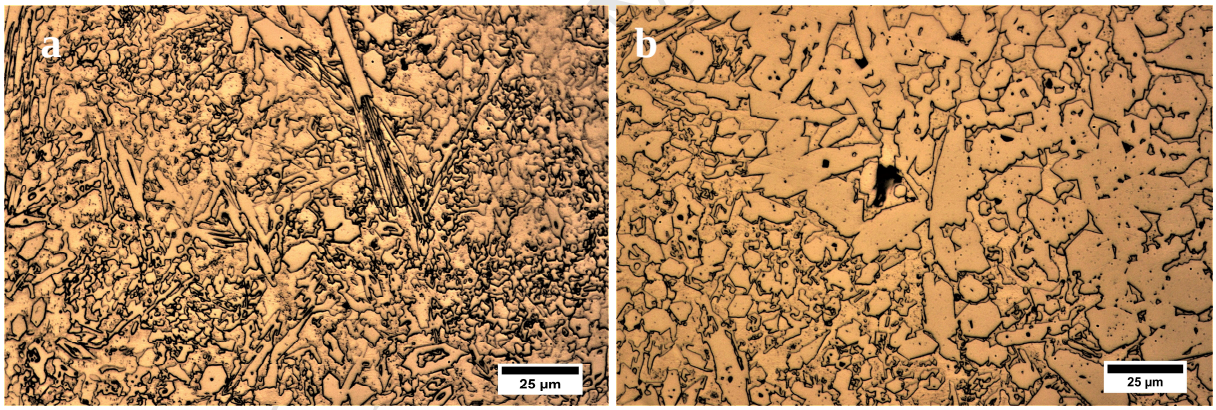

Fig. 3. Effects of sintering time on the carbide coarsening in samples, SPSed at 1050ºC for a) 10 and b) 15 min holding (sintering) time

In order to study the influence of sintering temperature on the porosity percentage of SPSed specimens, samples were SPSed at 950, 1000, 1050, 1075, and 1100˚C. Results showed that SPS at 1075 and 1100˚C is associated with the partial melting of consolidated samples. So, it appears that sintering should be conducted below 1075˚C. Fig. 4 shows the effects of sintering temperature on the porosity area fraction of sintered samples. Results show that 10 minutes of

sintering at 950 and 1000ºC is not enough to make solid bulk, with minimum interconnected porosities in the microstructure. One can see that an increase in the sintering temperature from 1000 to 1050ºC leads to a significant reduction of porosities in the SPSed sample. Sintering at 950˚C and 1000˚C result in the average porosity percentage 22.5 and 16%, while at 1050ºC, this is less than 3%. The presence of these porosities in the microstructure can obviously negatively affect mechanical properties of the samples. Based on the obtained results, sintering at 1050ºC for 10 minutes gives the best outcome.

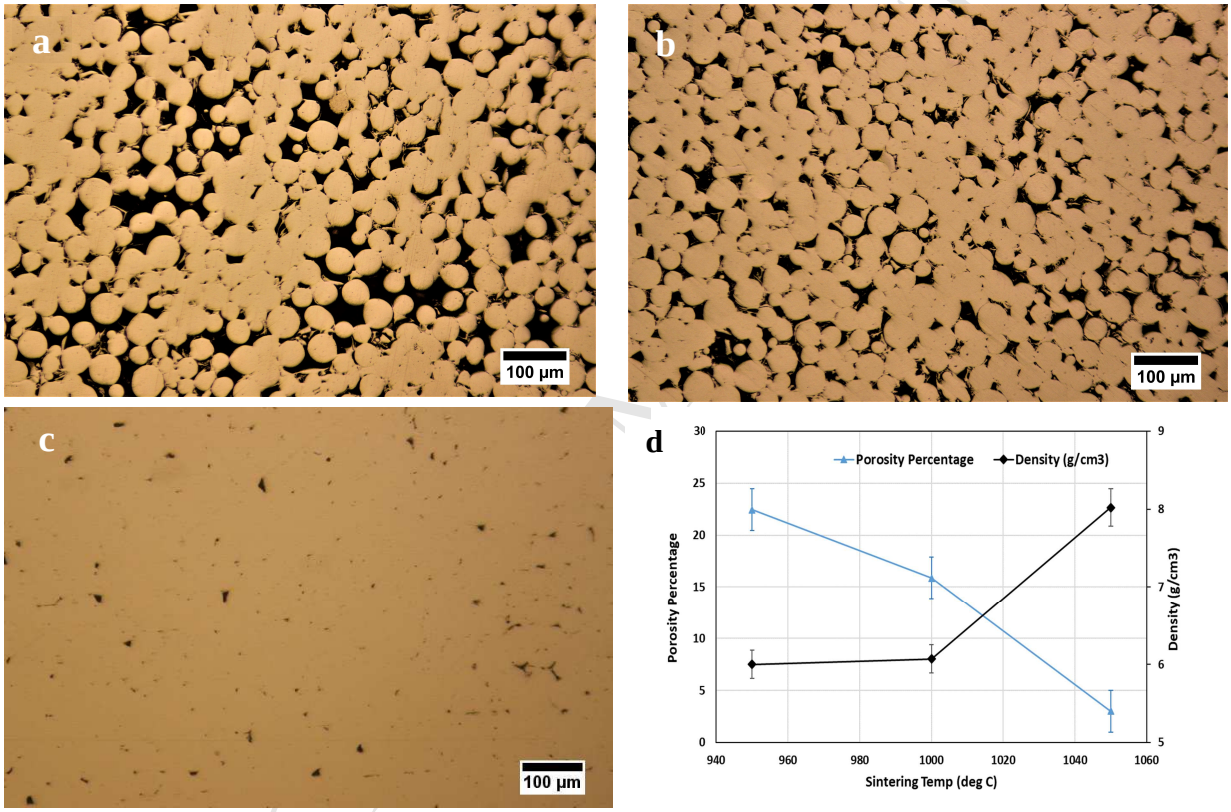

Fig. 4. Effects of sintering temperature a) 950, b) 1000, and c) 1050ºC on the d) porosity percentage and the density of consolidated samples.

XRD patterns of initial powder and samples sintered at temperatures 950 and 1050˚C are shown in Fig. 5. The peaks in all three patents are at similar degrees, inferring that no new phase (including intermetallic compounds) is formed during sintering (at least not within the detection limit of XRD). Stellite microstructure comprises a Co-based matrix with $M_{23}C_6$, M_7C_3, M_6C and WC carbides [24]. No WC, M_6C, and M_7C_3 were detected by XRD, implying

that the weight percentages of these phases are not enough to be detected by XRD. The majority of carbide phases in the microstructure belongs to $M_{23}C_6$. It is also noticeable that sintering has resulted in an overall reduction of peak intensities and peak broadening. This is comparatively more pronounced for the sample, sintered at 1050ºC. Both peak broadening and intensity reduction are indications of grain fragmentation/grain refinement and accumulation of lattice strain during sintering. Samples SPSed at 950 and 1050ºC have crystallite size of 39 and 31 nm respectively, whereas this is 65 nm in as-received powders.

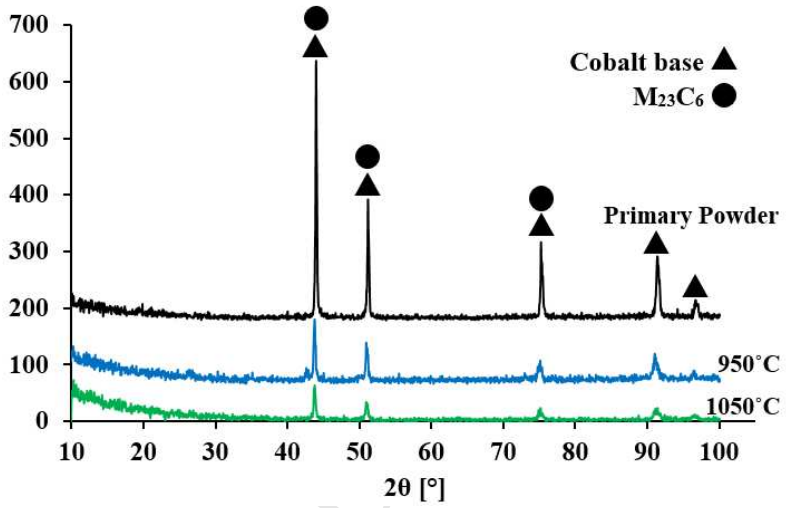

Fig. 5. XRD patterns of as-revised powders and samples, sintered at 950 and 1050˚C.

Typical microstructures of Stellite®-6 alloy SPSed at 1050ºC, are presented in Figs. 6 and 7. As can be seen, Stellite alloys have a Co-based matrix, essentially composed of intermingled complex dispersion of carbides. Carbides, present in the Stellite alloy, are reportedly mostly $M_{23}C_6$ and M_7C_3, with small amounts of M_6C and WC [24]. The latter is known to be a high-temperature carbide, while other carbides are more important for low and intermediate temperatures. Overall, intermingled complex dispersion of carbides (see Fig. 6) can enhance mechanical properties and improve wear/erosion resistance. EDS analyses of marked spots (given in Fig. 7) are presented in Fig. 8. EDS spectrum of spot 1 shows high concentration of Co, showing that spot 1 is the matrix. A high amount of Cr is detected in point 2, showing that this is a chromium-rich carbide. These chromium-rich carbides are mostly $M_{23}C_6$ carbides

[25]. The third analysis (spot 3) shows that the white phase is W-rich carbide. Fig. 9 shows elemental mapping of alloying elements in the microstructure, which is in accordance with the presented XRD and EDS results.

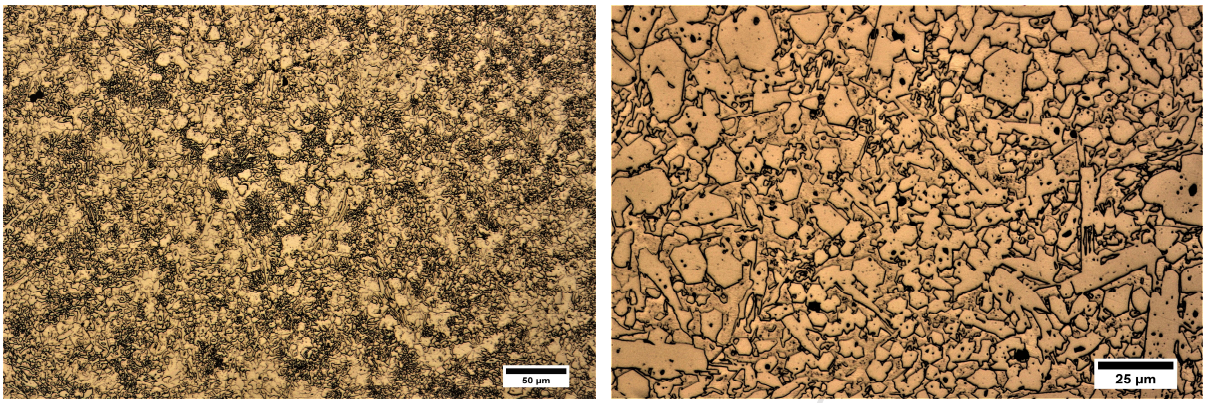

Fig. 6. Optical microscope images of microstructure of the sample, sintered at 1050ºC

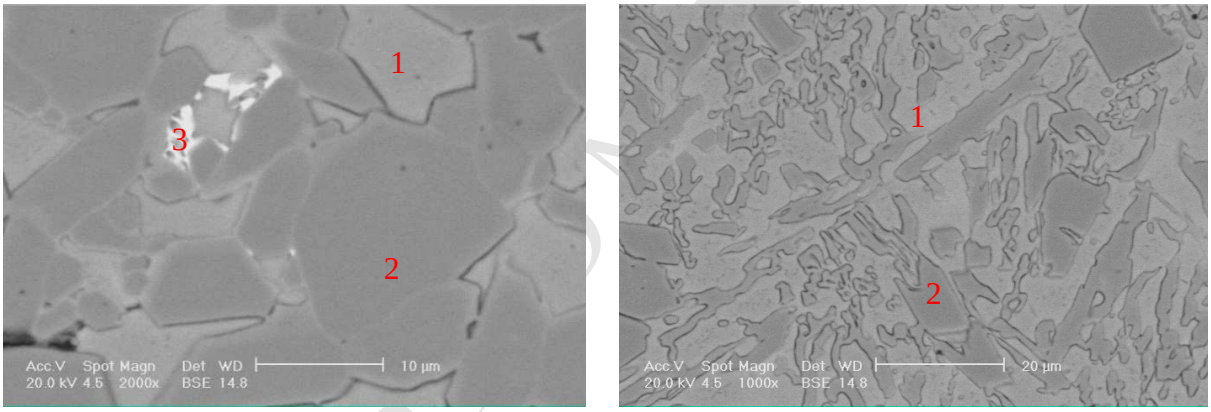

Fig. 7. BSE images of microstructure of the sample, sintered at 1050ºC

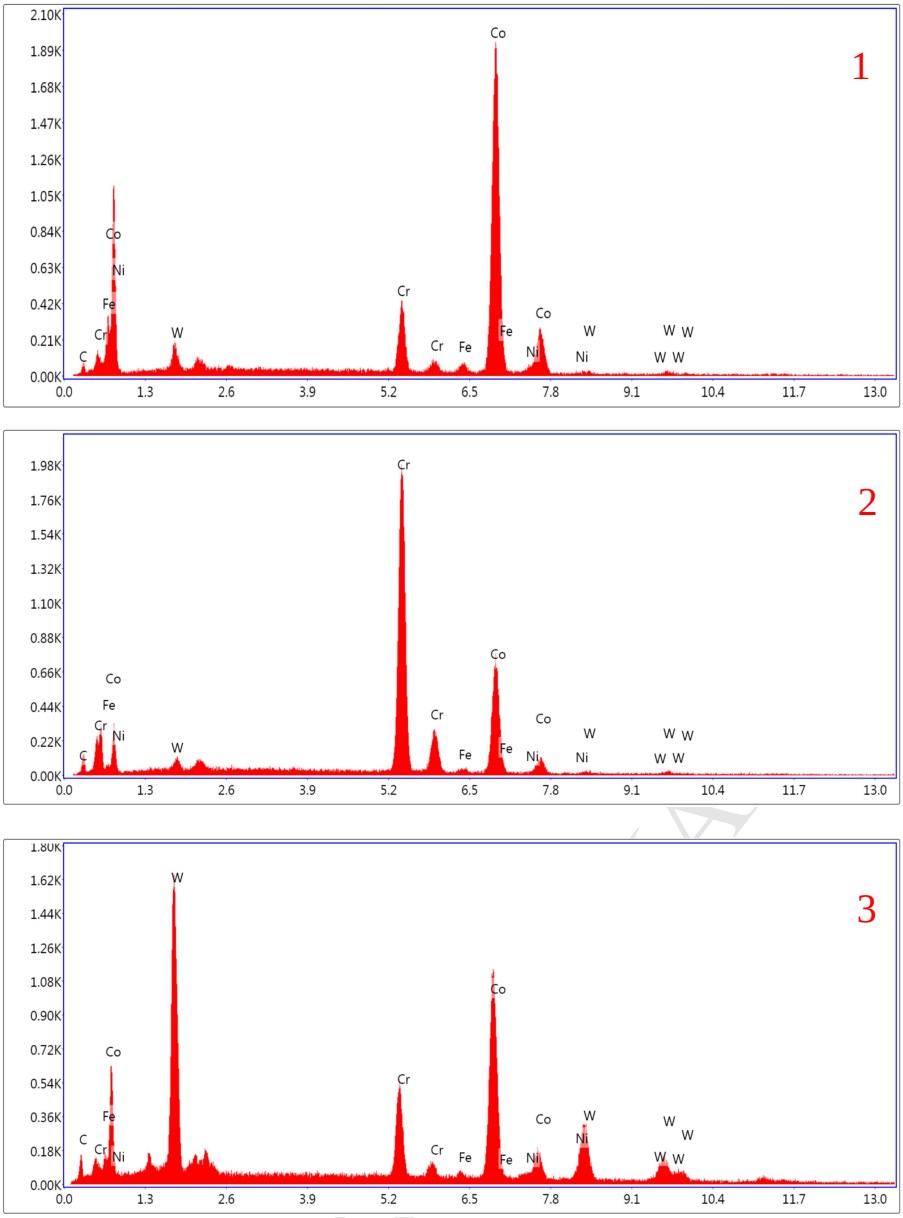

Element	Wt.%
Cr	8.2
Co	86.0
W	2.1
Fe	0.6
Ni	0.9
C	2.3

Element	Wt.%
Cr	52.2
Co	38.3
W	2.6
Fe	0.4
Ni	0.1
C	6.3

Element	Wt.%
Cr	9.6
Co	39.9
W	41.9
Fe	0.6
Ni	1.3
C	7.8

Fig. 8. EDS point analyses, taken from the spots, shown in Fig. 8.

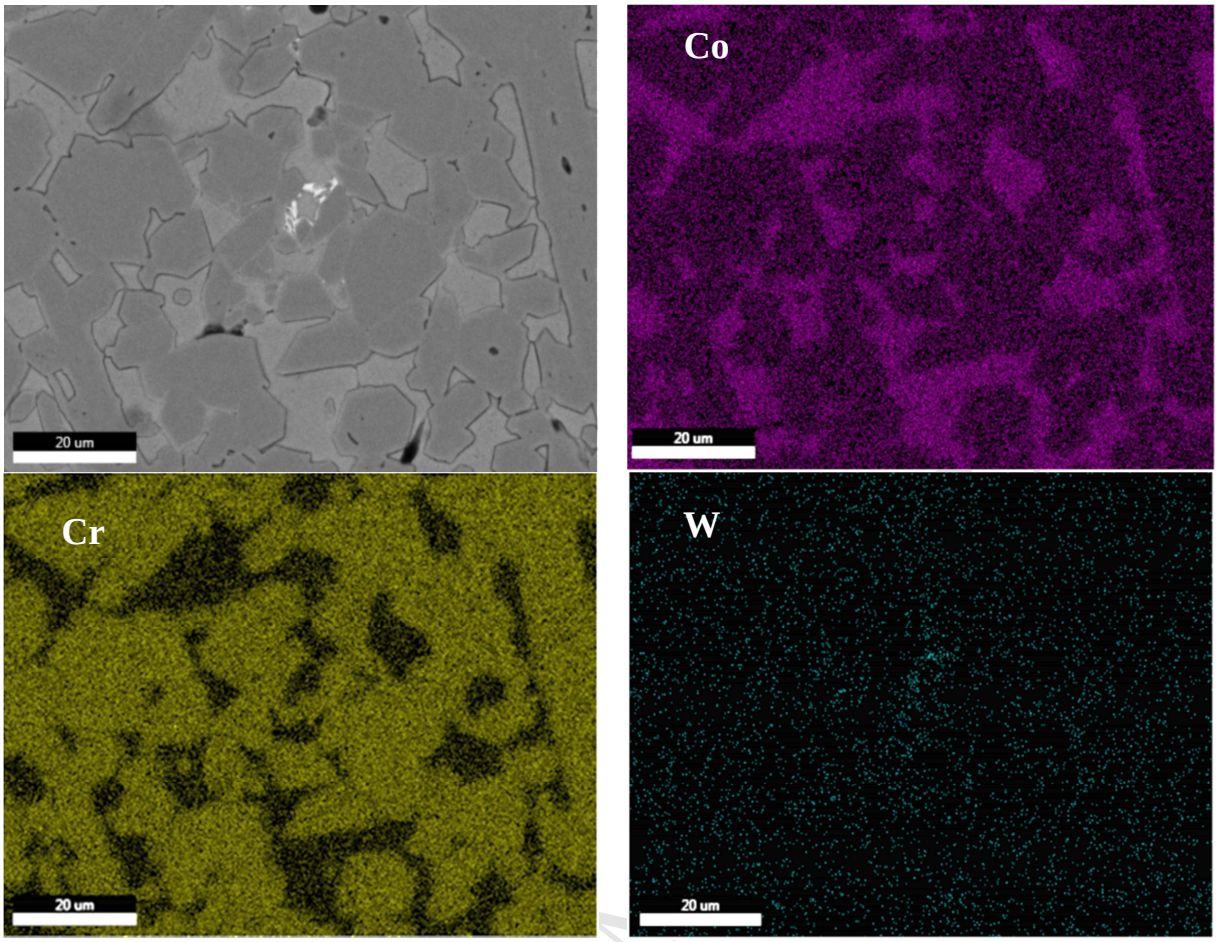

Fig. 9. Elemental mapping analysis from the sample, sintered at 1050°C

3.2. Mechanical properties of spark plasma sintered samples

The corresponding room and high temperature (650ºC) engineering compression stress–strain curves for SPSed samples at 950, 1000 and 1050˚C with strain rate of 4.5×10^{-4}/s are also shown in Fig. 10. There is a clear distinction between the mechanical properties of the sample, SPSed at 1050ºC and those of samples, sintered at lower temperatures (i.e. 950 and 1000ºC). The former shows remarkably better mechanical properties (yield and tensile strength as well as elongation). Samples, SPSed at 950 and 1000ºC, exhibit limited deformation before fracture, which obviously has to do with the fact that the sintering in these two temperatures is incomplete. Mechanical properties in structure with such high degrees of pore-connectivity are controlled by porosities rather than the material itself. On the contrary, mechanical properties of the sample, SPSed at 1050ºC, are controlled by complex primary

and secondary chromium-rich M_7C_3 and $M_{23}C_6$ carbides as well as tungsten-rich carbides [25]. The same goes for the Vickers hardness values, where the hardness values of SPSed samples at 950, 1000, and 1050ºC are 116, 158, and 510 $HV_{0.1}$ respectively. This can also be attributed to the reduced porosity with increased sintering temperature.

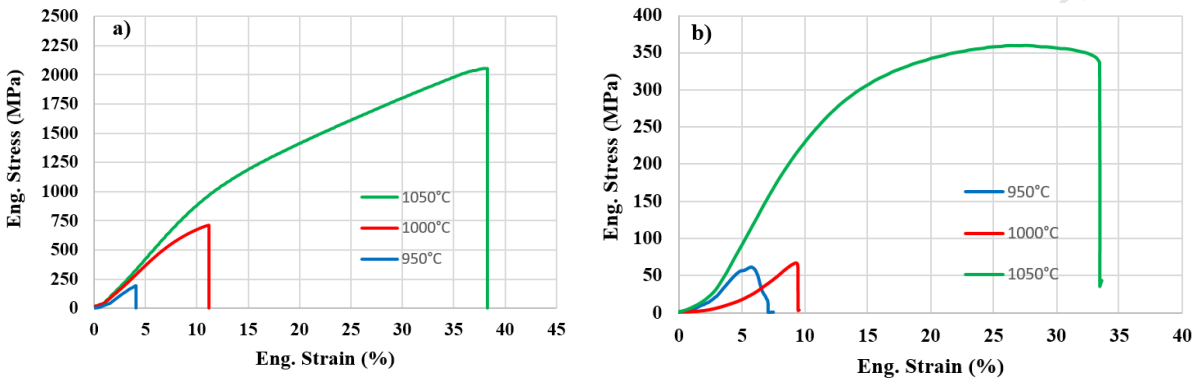

Fig. 10. Engineering Stress–strain compression curves of SPSed specimens at a) room temperature and b) 650ºC.

The tensile strength, hardness, and elongation values of SPSed Stellite®-6 alloy samples are compared with those of other manufacturing methods (see Table 2). Interestingly, samples produced by SPS show the highest yield strength and hardness, without any need for additional heat treatment. Such perfect combination of properties can be attributed to the relatively fast synthesis in SPS, which eliminates the risk of carbides coarsening/grain growth. In addition to that, low levels of porosities and intermingled nature of carbides certainly have positive contributions to the obtained mechanical properties.

Impact toughness test was also done on sintered specimens at room temperature. Results are shown in Table 2. Sample, sintered at 1050ºC for 10 min, showed the highest impact toughness value. But this is not a particularly high value. The microstructure of SPSed Stellite-6 essentially consists of an intermingled complex network of carbides in a matrix Co-based matrix (note Fig. 6). Carbides are inherently brittle and are known to be suitable positions for crack initiation and propagation [26]. Therefore, this relatively low value of impact toughness for optimum sample is not surprising. Also samples, sintered by SPS

technique, have certain amount of porosity. Porosities can also act as preferred crack nucleation sites, negatively affecting impact toughness of sintered alloys.

Table 2. Comparison between mechanical properties of Stellite-6 components, produced by SPS, PIM, casting, forging, and HIP (* Yield strength reported from Ref 9 is taken from stress-strain curves in this paper. The exact value of YS might be slightly different)

Production Method	Yield strength at RT (Mpa)	Yield strength at 650℃ (Mpa)	Hardness (HV)	Impact toughness (J)
SPS (at 950ºC)	191	57.78	116	1.3
SPS (at 1000ºC)	490	63.86	158	2.6
SPS (at 1050ºC)	885	220	510	8.3
PIM	~ 500 [9] *	-	428.25 [9]	-
Re-HIP	750 [10]	-	459.3 [10]	-
Casting	700 [10]	-	380-490 [25]	-
Forging (sheet)	635 [25]	-	-	-

Fig. 11 shows the fracture surface of samples, sintered at 950, 1000 and 1050˚C after compression test. Provided images are taken at low and high magnifications. The powdery nature of the fracture surface of samples, sintered at 950 and 1000˚C, is an indication that sintering at these two temperatures is incomplete. In the sample, sintered at 1000˚C, there is no sign of distinct powders. Interestingly, the fracture at the necks is typically a ductile fracture, confirmed by the presence of dimples on the fracture surface. By increasing sintering temperature to 1050˚C, there is no sign of isolated or interconnected particles at the fracture surface, which is in accordance with the comparatively lower porosity of this sample (see Fig. 4d). Contrary to samples, sintered at 950 and 1000ºC, in this case mechanical properties are controlled by the nature of material and not by the weak and poorly connected necks.

Fig. 12 shows the SEM fracture surface of specimens sintered at 1050˚C after fracture test. Microvoids and some porosities are evident in fracture surfaces (see red areas) that can certainly affect the impact toughness. As shown, the fracture mode is dominated by brittle

fracture leading to low impact toughness. Even though some local ductile fracture areas exist on the fracture surface, the fracture is obviously dominated by cleavage fracture [14, 27].

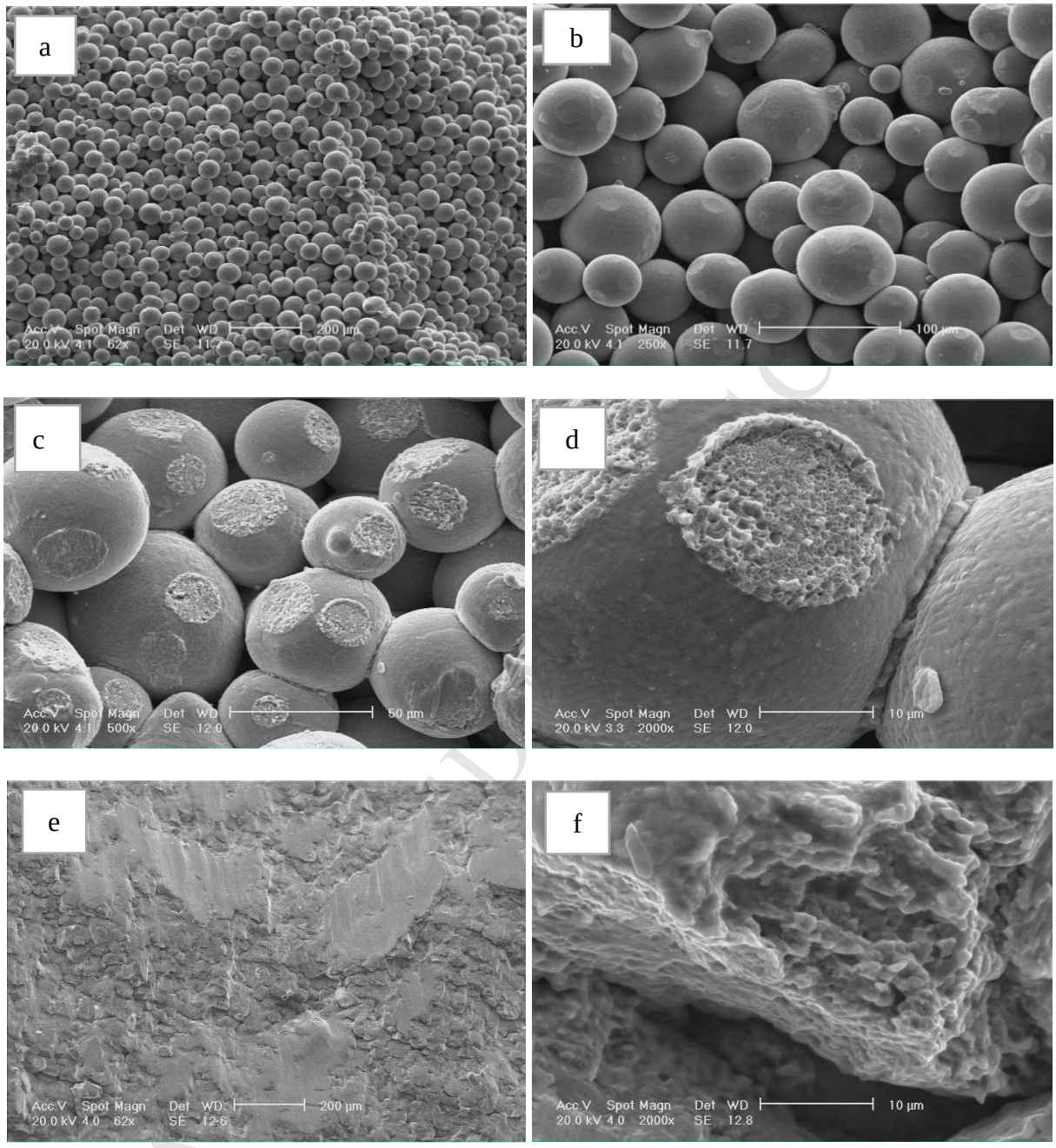

Fig. 11. Fracture surface morphologies (SEM/SE) of the samples sintered at different temperatures; sintered at (a and b) 950°C, (c and d) 1000°C and (e and f) 1050°C after compression test.

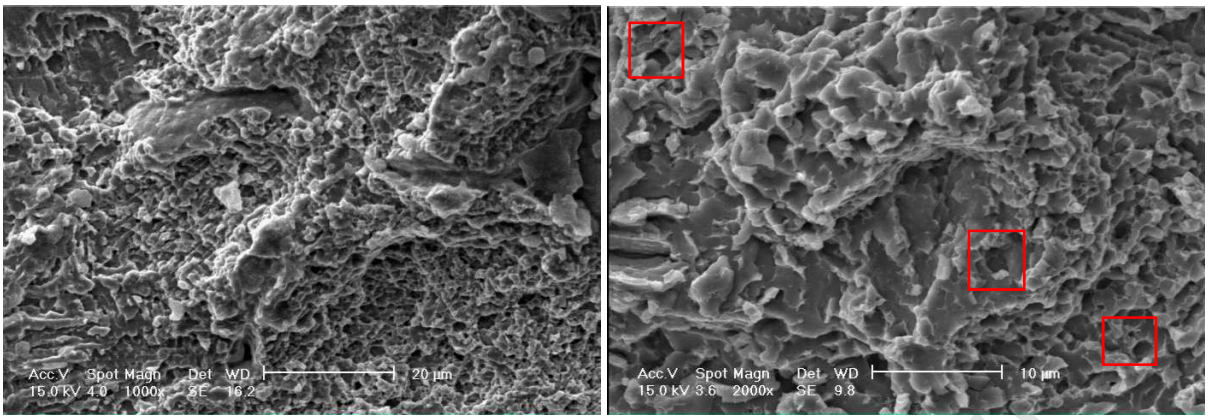

Fig. 12. Fracture surface (SEM/SE) of samples sintered at 1050°C (optimum condition) after impact test at room temperature (highlighted areas show microvoids/porosities)

4. Conclusions

This study aims at investigating the effects of spark plasma sintering (SPS) on the microstructure and mechanical properties of cobalt-based Stellite®-6 superalloy. Results showed that it was not possible to achieve a complete pore-free specimen with SPS. The minimum porosity (roughly 3%) and the highest densification, can be obtained after 10 min of sintering at 1050ºC. Higher holding time results in the coarsening of chromium carbides in the microstructure. Also, decreasing sintering temperature is associated with an incomplete sintering, such a way that isolated or poorly connected powders can be easily seen in the microstructure. EDS results showed that the main secondary phase is chromium-rich carbide. The XRD results also confirmed the presence of chromium carbides. It is also seen that sintering is associated with XRD peaks broadening, which is an indication of grain fragmentation and formation of smaller crystallites. Mechanical properties of the optimum specimen are much higher than those obtained by other P/M methods.

5. Data Availability

The raw data required to reproduce these findings are available to download from www.sciencedirct.com. The processed data required to reproduce these findings are available to download from www.sciencedirect.com.

6. References

[1] S.H. Mousavi Anijdan, A. Bahrami, A new method in prediction of TCP phases formation in superalloys, Mater. Sci. Eng. A 396 (1-2) (2005) 138-142. https://doi.org/10.1016/j.msea.2005.01.012.

[2] J. Yao, Z. Li, B. Li, L.Yang, Characteristics and bonding behavior of Stellite 6 alloy coating processed with supersonic laser deposition, J. Alloys and Compd. 661 (15) (2016) 526-534. https://doi.org/10.1016/j.jallcom.2015.11.077.

[3] F.Madadi, F.Ashrafizadeh, M.Shamanian, Optimization of pulsed TIG cladding process of stellite alloy on carbon steel using RSM, J. Alloys and Compd. 510 (1) (2012) 71-77. https://doi.org/10.1016/j.jallcom.2011.08.073.

[4] A.Gholipour, M.Shamanian, F.Ashrafizadeh, Microstructure and wear behavior of stellite 6 cladding on 17-4 PH stainless steel, J. Alloys and Compd. 509 (14) (2011) 4905-4909. https://doi.org/10.1016/j.jallcom.2010.09.216.

[5] H. Lavvafi, M.E. Lewandowski, D. Schwam, J.J. Lewandowski, Effects of surface laser treatments on microstructure, tension, and fatigue behavior of AISI 316LVM biomedical wires, Mater. Sci. Eng. A 688 (2017) 101-113. https://doi.org/10.1016/j.msea.2017.01.083.

[6] S.H. Mousavi Anijdan, H.R. Jafarian, A. Bahrami, Microstructural characteristics of nano-structured Fe-28.5 Ni steel by means of severe plastic deformation, IOP Conference Series: Mater. Sc. Eng. 194 (2017) 012051. https://doi:10.1088/1757-899X/194/1/012051.

[7] P. Budzyńskia, M. Kamińskia, M. Wiertelb, K. Pyszniakb and A. Droździelb, Mechanical Properties of the Stellite 6 Cobalt Alloy Implanted with Nitrogen Ions, J. Acta Physica Polonica A., 132 (2017) 203-205. https:// doi:10.12693/APhysPolA.132.203.

[8] U. Malayoglu, A. Neville, Comparing the performance of HIPed and Cast Stellite 6 alloy in liquid–solid slurries, Wear, 255 (2003) 181–194. http://dx.doi:10.1016/S0043-1648(03)00287-4.

[9] H. Ö. Gülsoy, Ö. Özgün, S. Bilketay, Powder injection molding of Stellite 6 powder: Sintering, microstructural and mechanical properties, Mater. Sci. Eng. A 651 (2016) 914–924. http://dx.doi.org/10.1016/j.msea.2015.11.058.

[10] R. Ahmed, A. Ashraf, M. Elameen, N.H. Faisal, A.M. El-Sherik, Y.O. Elakwah, M.F.A. Goosen, Single asperity nanoscratch behaviour of HIPed and cast Stellite 6 alloys, Wear, 312 (2014) 70–82. http://dx.doi.org/10.1016/j.wear.2014.02.006.

[11] F. Rosalbino, G. Scavino, Corrosion behaviour assessment of cast and HIPed Stellite 6 alloy in a chloride-containing environment, Electrochimica Acta, 111 (2013) 656–662. http://dx.doi.org/10.1016/j.electacta.2013.08.019.

[12] S. Sugiyama, Y. Sugawara, M. Kimura, K. Asari, T. Yoshida, H. Taimatsu, Consolidation of Stellite and Its Bonding to Stainless Steel by Spark Plasma Sintering, J. the Japan Soc. of Powder and Powder Metallurgy, 45 [7] (1998) 675-679. https://doi.org/10.2497/jjspm.45.675.

[13] B.A. Obadele, O.O. Ige, P.A. Olubambi, Fabrication and characterization of titanium-nickel-zirconia matrix composites prepared by spark plasma sintering, J. Alloys and Compd. 710 (2017) 825-830. http://dx.doi.org/10.1016/j.jallcom.2017.03.340.

[14] M.I. Makena, M.B Shongwe, M.M. Ramakokovhu, P.A Olubambi, Effect of sintering parameters on densification, corrosion and wear behaviour of Ni-50Fe alloy prepared by spark plasma sintering, J. Alloys and Compd. 699 (2017) 1166-1179. http://dx.doi.org/10.1016/j.jallcom.2016.12.368.

[15] M.B. Shongwe, M.M. Ramakokovhu, S. Diouf, M.O. Durowoju, B.A. Obadele, R. Sule a, M.L. Lethabane, P.A. Olubambi, Effect of starting powder particle size and heating rate on spark plasma sintering of Fe-Ni alloys, J. Alloys and Compd. 678 (2016) 241-248. http://dx.doi.org/10.1016/j.jallcom.2016.03.270.

[16] T. Borkar, R. Banerjee, Influence of spark plasma sintering (SPS) processing parameters on microstructure and mechanical properties of nickel, Mater. Sci. Eng. A 618 (2014) 176–181. http://dx.doi.org/10.1016/j.msea.2014.08.070.

[17] X. Song, X, Liu, J. Zhang, Neck Formation and Self-Adjusting Mechanism of Neck Growth of Conducting Powders in Spark Plasma Sintering, J. Am. Ceram. Soc. 89 [2] (2006) 494–500. https://doi.org/10.1111/j.1551-2916.2005.00777.x.

[18] A. Azarniya, A. Azarniya, S. Sovizi, H.r Madaah Hosseini, T. Varol, A. Kawasaki, S. Ramakrishna, Physicomechanical properties of spark plasma sintered carbon nanotube-reinforced metal matrix nanocomposites, Progress in Materials Science, 90 (2017) 276–324. http://dx.doi.org/10.1016/j.pmatsci.2017.07.007.

[19] C.F. Tang, F. Pan, X.H. Qu, C.C. Jia, B.H. Duan, X.B. He, Spark plasma sintering cobalt base superalloy, strengthened by Y–Cr–O compound through high-energy milling, J. of Mat. Processing Technology, 204 (2008) 111-116. http://dx.doi:10.1016/j.jmatprotec.2007.10.084.

[20] G.K. Williamson, W.H. Hall, X-ray line broadening from filed aluminium and wolfram, Acta Metall., 1 (1953) 22‑31. https://doi.org/10.1016/0001-6160(53)90006-6.

[21] M.A. Sokolov, J.D. Landes, G.E. Lucas, Small Specimen Test Techniques: Fourth Volume, ASTM STP1418, USA, 2002.

[22] M.B. Shongwe, S. Diouf, M.O. Durowoju, P.A. Olubambi, Effect of sintering temperature on the microstructure and mechanical properties of Fe-30%Ni alloys produced by spark plasma sintering, J. Alloys and Compd. 649 (2015) 824-832. https://doi.org/10.1016/j.jallcom.2015.07.223.

[23] Y. Ning, P.C. Patnaikb, R. Liua, M.X. Yaoc, X.J. Wu, Effects of fabrication process and coating of reinforcements on the microstructure and wear performance of Stellite alloy composites, Mater. Sci. Eng. A 391 (2005) 313–324. https://doi.org/10.1016/j.msea.2004.08.083.

[24] W.S. da Silva, R.M. Souza, J.D.B. Mello, H. Goldenstein, Room temperature mechanical properties and tribology of NICRALC and Stellite casting alloys, Wear, 271 (2011) 1819–1827. https://doi.org/10.1016/j.wear.2011.02.030.

[25] M.J. Donachie, S.J. Donachie, Understanding Superalloy Metallurgy, in: M.J. Donachie, S.J. Donachie (Eds.), Superalloys A Technical Guide, Second Ed., ASM International Materials Park, OH 44073-0002 USA, 2002, pp. 25-39.

[26] Y.H. Yang, J.J. Yu, X.F. Sun, T. Jin, H.R. Guan, Z.Q. Hu, Investigation of impact toughness of a Ni-based superalloy at elevated temperature, Materials and Design, 36 (2012) 699–704. https://doi:10.1016/j.matdes.2011.11.067.

[27] M. Kiani Khouzani, A. Bahrami, A. Eslami, Metallurgical aspects of failure in a broken femoral HIP prosthesis, Eng. Fail. Ana., 90 (2018) 168-178. https://doi.org/10.1016/j.engfailanal.2018.03.018.

- Spark plasma sintering of Stellite superalloy is investigated
- Optimum mechanical properties can be obtained after sintering at 1050ºC for 10 min
- Correlations between microstructure and sintering parameters are discussed